We are IntechOpen, the world's leading publisher of Open Access books Built by scientists, for scientists

6,900
Open access books available

185,000
International authors and editors

200M
Downloads

Our authors are among the

154
Countries delivered to

TOP 1%
most cited scientists

12.2%
Contributors from top 500 universities

WEB OF SCIENCE™

Selection of our books indexed in the Book Citation Index in Web of Science™ Core Collection (BKCI)

Interested in publishing with us?
Contact book.department@intechopen.com

Numbers displayed above are based on latest data collected.
For more information visit www.intechopen.com

Chapter 15

Pyridinium-Based Ionic Liquids — Application for Cellulose Processing

Elena S. Sashina and Dmitrii A. Kashirskii

Additional information is available at the end of the chapter

http://dx.doi.org/10.5772/59286

1. Introduction

Over the last two decades new direct solvents for cellulose and other natural polymers have been actively explored; these are ionic liquids (ILs). The unique properties of this new class of compounds allow the use of ILs in various fields of science and technology, among which the use of ILs as the reaction medium for biomass processes occupies an important place [1-3], especially for cellulose dissolution [4-13], and the dissolution of other natural polymers [14], and produces from their solutions new biodegradable materials, including films, fibres and membranes [15].

On the whole, imidazolium-, ammonium-and pyridinium-based ILs can be used for cellulose dissolution (Figure 1). Imidazolium ILs are studied here in great detail, but the comparisons between the cost of synthesis, toxicity [16-18] and dissolving power [4, 6] of the three classes of ILs shows pyridinium-containing salts to be of most benefit. The most effective salts have a pyridinium ring with position 1,3 of alkylic substituents [6, 7].

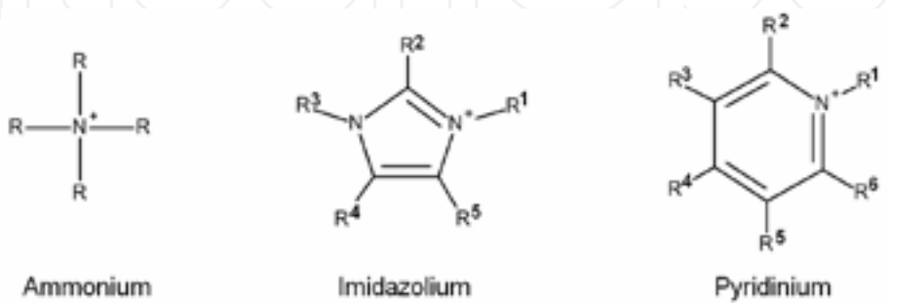

Figure 1. IL cations suitable for cellulose dissolution

INTECH
open science | open minds

© 2015 The Author(s). Licensee InTech. This chapter is distributed under the terms of the Creative Commons Attribution License (http://creativecommons.org/licenses/by/3.0), which permits unrestricted use, distribution, and eproduction in any medium, provided the original work is properly cited.

The important feature of ILs is the possibility of selecting the cation-anion pairs for the purposeful synthesis of solvents with desirable properties in technology. In view of the large numbers of ILs available, the selection of ionic solvents out of all the possible cation-anion pairs is a big problem. To make a reasonable selection it is important to understand the relationship between the structure, physicochemical properties, and dissolving power of ILs.

2. Experimental

2.1. Quantum-chemical calculations

Quantum-chemical calculations were performed using the Gaussian 03 program by HF/3-21G(d) and HF/6-31G(d) methods [7]. As the IL models were used the ionic pairs which they contained associated cation and anion. For the cellulose model, we took the cellotetraose (i.e., saccharide consisting of four glycoside units). The interaction energy of the IL's cation-anion pairs, E_p, was calculated as a difference: the energy of the cation-anion complex, E_{ca}, minus the sum of the energies of the cation, E_c, and the anion, E_a:

$$E_p = 2625.5 \bullet \{E_{ca} - (E_c + E_a)\},$$

where 2625.5 is the conversion factor of the Hartree energy (atomic units) in kJ mol^{-1}.

2.2. ^{1}H-NMR spectroscopy

An analysis of the chemical shifts was carried out by the ^{1}H-NMR spectra obtained with the Bruker Avance II Plus 700 MHz spectrometer (at an operating frequency of 700 MHz) at a temperature of 27 °C. For the preparation of the samples, a sample of the IL (19 – 27 mg) was dissolved in $CDCl_3$ (0.65 mL, δ=7.240 ppm). Solutions of cellulose with ILs were investigated using the $CDCl_3$ (δ=7.240 ppm). TMS (δ=0) was used as the internal standard [19].

2.3. Thermal analysis

Differential scanning calorimetry (NETZSCH-Gerätebau GmbH Thermal Analysis DSC 204), thermogravimetry methods (F. Paulik J.Paulik L. Erdey system) and Boëtius heated stage (VEB Wagetechnik Rapido) were used for the thermal analysis [20]. The conditions of the experiment are shown in Table 1. For the Boëtius heated stage: the samples were placed on a microscope slide and the cover glass, and these were added to the heated stage, and the melting process was observed with the aid of a microscope PHMK 05 (with an increasing of 16 times). For the melting point, the state of the total loss of the sharp edges of the salts' crystals is taken.

2.4. Gas chromatography–mass spectrometry

The IL samples were identified on the Shimadzu GCMS-QP2010 Plus. For this equipment the FFNSC 1.2 and NIST08 libraries were used. The main analysis conditions involved a capillary

Method	Temperature range, ºC	Heating rate, deg/min	Sample mass, mg	Atmosphere
DSC	–80 ÷ 350	10	7.80 – 8.50	Nitrogen
DTG	20 ÷ 200	7.9	~ 90.00	Air
Boëtius heated stage	20 ÷ m.p.	10	7.00 – 10.00	Air

Table 1. Conditions of the thermal analysis of ionic liquids [20].

chromatographic column (30 m), a stationary phase SLB-5ms, the carrier gas was helium, and the evaporator temperature was 200 °C. The thermostat columns had a temperature range of 40 °C (for five minutes) to 280 °C, a heating rate of 10 deg/min and exposure for 15 minutes. The detector of the mass spectrometer with the quadrupole mass analyser had a detection range of *M*/*Z* 40 – 450 Da. The delay of the start of the registration (for the cut-off of the solvent) was 2.2 min. For the sample preparation, IL crystals (5 mg) were dissolved in ethanol (1:200), 1 μL of solution was injected into the evaporator chromatograph with a microsyringe.

2.5. Fourier transform infrared spectroscopy

The FTIR spectra of the samples were recorded on a Nicolet 6700 FT-IR from Thermo Scientific. The resolution was 0.5 cm^{-1}. The spectra were recorded at room temperature using an NXR FT-Raman module.

2.6. Dissolution of cellulose with ILs

Cellulose was added to the solvent after the complete dissolution of the previous sample (in this case the solution was transparent to light and did not contain any undissolved cellulose fibres visible under the microscope). To determine the maximum dissolving power of the ILs, the dissolution was carried out for not less than 12 hours with a constant stirring and temperature control using the magnetic stirrer. The calculation of the dissolved cellulose concentration was given by the formula:

$$D = \frac{m_1}{m_1 + m_2} \bullet (100 - W),$$

where D is the concentration of the cellulose solution with ILs, wt%; m_1 and m_2 are the mass of the cellulose and ILs, respectively, g; W is the water content of the cellulose, wt% [7].

2.7. Optical microscopy

A microscopic examination of the samples was carried out using a laboratory microscope Euler Science 670TD. A digital camera was used DCM 510 (5-MPix, 1/2'' CMOS) with a maximum resolution of 2592×1944, and a sensitivity of 0.90 V/lux-sec at 550 nm.

2.8. Degree of polymerization of cellulose

To determine the degree of polymerization (DP) of the initial cellulose and the regenerated polymer (i. e. the film obtained from solution of cellulose with ILs) from an aqueous solution of cadmium-ethylenediamine complex (cadoxene), containing 29 wt% ethylenediamine. The cellulose was used at the following concentrations (D): 0.1, 0.2, 0.3, and 0.4 wt%. We used an Ostwald viscometer (the capillary of which had an internal diameter of d=0.99 mm), analytical balance (with a precision of four decimal places) and a thermostat at $U15^C$ MLW (bath temperature: 20 °C). Using the time of the expiration (in sec.) of pure cadoxene (τ_0) and the solution (τ_i) the relative viscosity was calculated:

$$\eta_r = \frac{\tau_i}{\tau_0}.$$

The specific viscosity was determined from the relationship: $\eta_s = \eta_r - 1$, and the reduced viscosity: $\eta_i = \eta_r/D$. The intrinsic viscosity [η] found by graphical extrapolation to the value of D=0 using the software package Origin 9.0 was:

$$\lim_{D\to 0} \frac{\eta_s}{D} = \lim_{D\to 0} \frac{\ln \eta_r}{D}.$$

The intrinsic viscosity is related to the DP value for a given diameter of the viscometer capillary as $[\eta]=7\ 10^{-3}\ DP^{0.9}$, therefore

$$DP = \left(\frac{[\eta]}{0.007}\right)^{\frac{1}{0.9}}.$$

3. Physical and chemical properties of pyridinium-based ionic liquids

3.1. Theoretical studies of the 1-alkylpyridinium- and 1-alkyl-3-methylpyridinium-based salts, and their structural features

Quantum chemical calculations can give an insight into geometry and the charge distribution of organic compounds. We studied pyridinium derivatives with different alkylic lengths and the numbers of the substituents of the ring have different anions.

3.1.1. Features of the structures of the 1-substituted pyridinium-based ILs

Theoretically, the optimal geometry of the studied pyridinium derivatives can be determined based on the results of quantum chemical calculations (method HF/3-21G(d)) as coordinates of the minimum (minima) on the potential energy surface, PES. As an example, Figure 2 shows the function of a cation-anion pair's interaction energy, E_p, the distances between the cation and anion $r_{(H2\cdots Cl)}$, the torsion angle Θ between the atoms N, C^2, H^2 of 1-methylpyridinium rings, and the chloride-anion Cl for $[C_1Py]Cl$ [11].

http://dx.doi.org/10.5772/59286

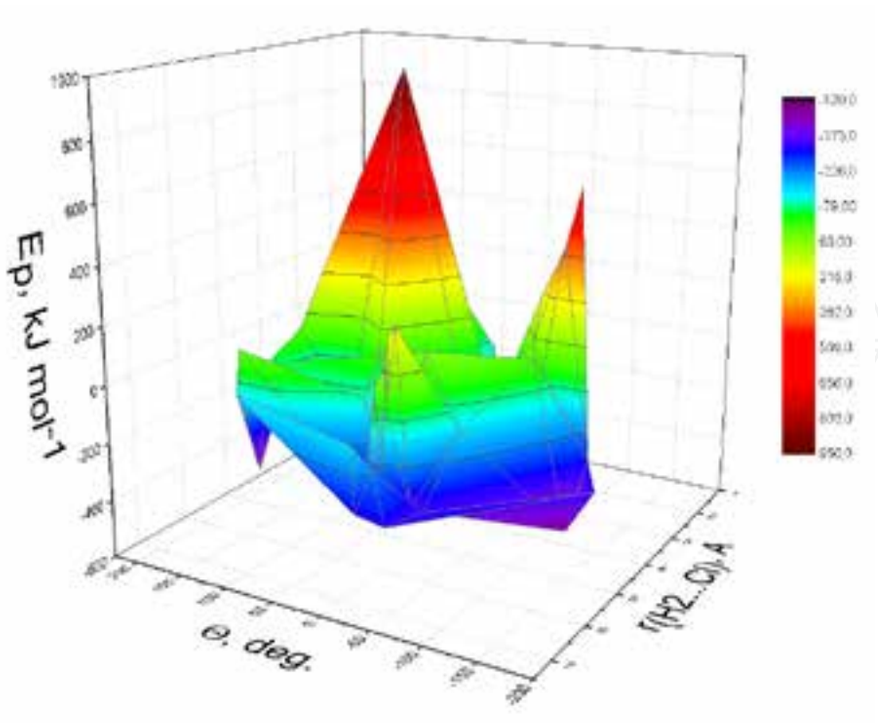

Figure 2. PES for $[C_1Py]Cl$

The minimum of the E_p value corresponds to the location of the anion near the atom H^2 (the most electron-deficient atom) of the ring and H^6 of the aliphatic chain (Fig. 3A). At the point of the global minimum, the torsion angle between atoms N, C^2, H^2, and Cl becomes 0°, since the ring of pyridine and its derivatives have a rigid and almost planar structure, and the anion is located on the same plane. The energy of the complex is -519 kJ mol^{-1}, $r_{(H2\cdots Cl)}$ 2.17 Å. There are local minima with energy E_p= -367.06 kJ mol^{-1} at $r_{(H2\cdots Cl)}$=5.87 Å, and Θ=23.38° (Fig. 3B) and-363.45 kJ mol^{-1} at $r_{(H2\cdots Cl)}$=2.73 Å and Θ=10.87° (Fig. 3C). The least probable relative positions of anion and cation correspond to the maximum positive value of E_p=+948.00 at $r_{(H2\cdots Cl)}$=3.08 Å, Θ=90.61°, (Fig. 3D). In this case the anion is located above the plane of the ring. A positive value of E_p is due to the repulsion of the anion by the π-bonds of the pyridinium ring saturated with electron density.

The 1-substituted formation from pyridine molecule (Py) leads to minimal changes in the bond lengths and angles on the pyridinium ring (Table 2). It indicates that these structures have rigid and high symmetry geometry [21]. Appreciable differences were noted only in the angle values of α and β for the 1-substituted pyridinium compared with Py.

Calculations show that the distance between the anion and the cation increases slightly with the increasing length of the cationic substituent, but the distance between the anions and cationic substituents (atom $H^{1'}$) is reduced. So, in a series of C_1–C_6 the distance between the chloride anion and the nearest H^2 atom of the ring increases (2.190 → 2.225 Å). Starting from C_3 the anion approaches the substituents, and the distance between the anion and the nearest atom H^2 of the cationic substituent is shortened (2.624 ← 2.525 Å). In the C_0–C_4 series, as in the case of the imidazolium-based ILs [22], there is a tendency for a gradual decrease in the

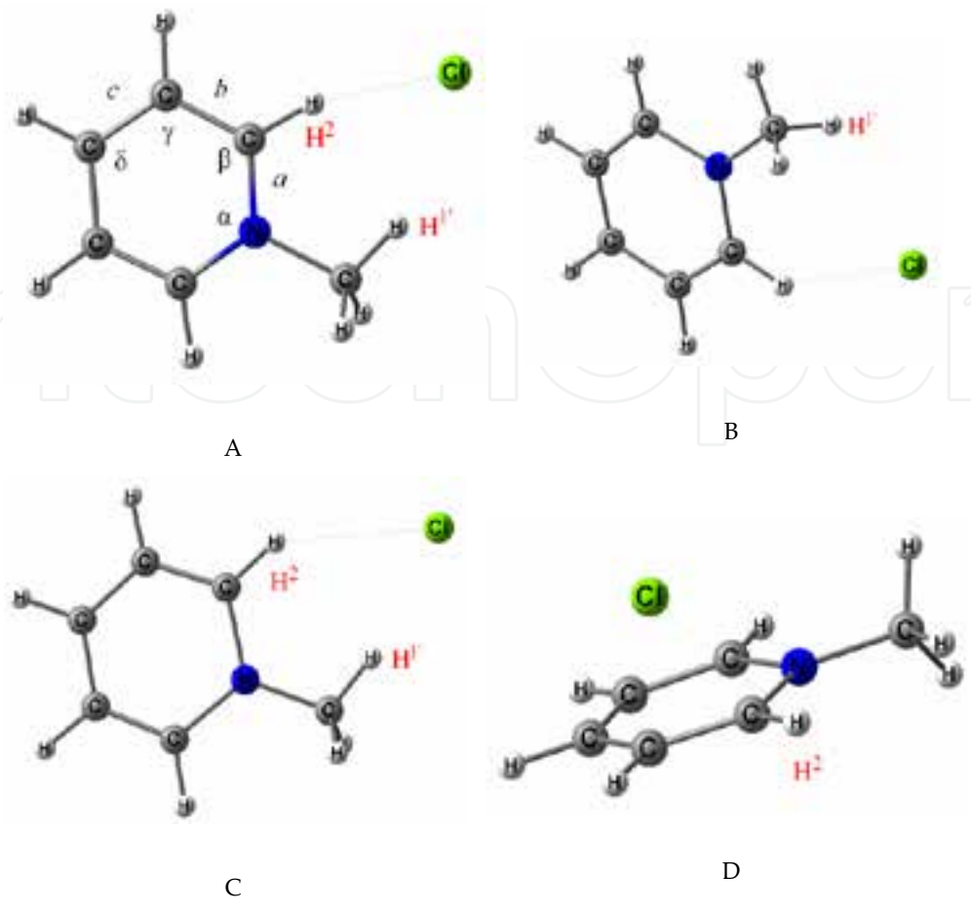

Figure 3. Models of $[C_1Py]Cl$ with different arrangements of the anion around the cation, calculated by HF/3-21G(d)

interaction energy between the cation and the anion; this trend correlates with the experimentally observed decrease in the dissolving power toward cellulose and other higher plants (Table 3). It can be assumed that this leads to changes in the degree of the ordering of the ionic liquid (density fluctuation) manifested as the appearance of polar and nonpolar domains [23]. In any case, increases in the length of the substituent leads to a decrease in the density of the polar component.

	Parameters:	Py		[HPy]Cl	$[C_1Py]Cl$	$[C_2Py]Cl$	$[C_3Py]Cl$	$[C_4Py]Cl$	$[C_5Py]Cl$	$[C_6Py]Cl$	[APy]Cl	[BzPy]Cl
		Calc.	Ref. [21]									
Geometry	*a*	1.321	1.335	1.325	1.331	1.333	1.334	1.334	1.331	1.333	1.331	1.331
	b	1.385	1.381	1.377	1.388	1.386	1.384	1.384	1.387	1.385	1.386	1.386
	c	1.384	1.379	1.387	1.374	1.376	1.377	1.377	1.375	1.377	1.375	1.375
	α	117.704	117.670	122.744	121.34	121.21	121.19	121.06	121.06	121.21	121.28	121.14
	β	123.607	122.990	120.268	119.96	120.08	120.17	120.20	120.21	120.11	120.07	120.19
	γ	118.229	118.840	118.285	119.48	119.44	119.42	119.41	119.41	119.41	119.39	119.39

http://dx.doi.org/10.5772/59286

	Parameters:	Py		[HPy]Cl	[C_1Py]Cl	[C_2Py]Cl	[C_3Py]Cl	[C_4Py]Cl	[C_5Py]Cl	[C_6Py]Cl	[APy]Cl	[BzPy]Cl
		Calc.	Ref. [21]									
	δ	118.624	118.650	120.149	119.46	119.44	119.41	119.40	119.39	119.45	119.48	119.39
	$r_{(H2\cdots Cl)}$				2.190	2.201	2.203	2.205	2.221	2.225	2.221	2.208
	$r_{(Cl\ldots H1')}$			1.821	2.464	2.575	2.624	2.623	2.525	2.592	2.537	2.564
Charges	q_{Cl}			-0.746	-0.852	-0.862	-0.864	-0.864	-0.852	-0.866	-0.866	-0.852
	q_N	-0.515		-0.685	-0.603	-0.604	-0.605	-0.605	-0.603	-0.611	-0.607	-0.602
	q_{H^2}	0.202		0.293	0.363	0.364	0.363	0.363	0.357	0.365	0.359	0.361
	$q_{H^{1'}}$			0.431	0.325	0.305	0.304	0.305	0.317	0.299	0.314	0.314
	E_p			-436.965	-369.919	-367.434	-364.033	-362.158	-363.133	-365.211	-365.149	-866.474
	$\vec{\mu}$, D	2.31	2.20 [24]									

Table 2. The main geometrical parameters, the effective charge values on the atoms, q, the cation-anion interaction energy, E_p (kJ mol^{-1}), and the dipole moment, (D), of the models Py, 1-substituted pyridinium-based chlorides, calculated by HF/6-31G(d) [11]

Solvents	Dissolving power
[HPy]Cl	biomass poplar 80 mg g^{-1}*, pine 60 mg g^{-1}* at 60°C [25]
[C_2Py]Cl	cellulose ~ 5 %, at 90 – 100 °C [26]
[C_4Py]Cl	biomass poplar 30 mg g^{-1}* at 60 °C [25]
[APy]Cl	biomass poplar mg g^{-1}* at 60 °C [25]; cellulose ~ 5 % at 105 – 110 °C [26]
[APy]Br	biomass poplar 5 mg g^{-1}* at 60 °C [25]
[BzPy]Cl	cellulose ~ 5 % at 110 – 115 °C [26]

* by dilution in DMSO (1:2).

Table 3. The solubility biomasses with 1-alkylpyridinium-based salts, according to the works [25,26]

Regardless of the kind of anion (we examined 1-methylpyridinium cation-based models of salts with chloride-anion, bromide-anion and acetate-anion, Figure 4),these have been placed near the pyridinium ring H^2 atom, which is characterized by low electron density (Table 4). The bond lengths of the pyridinium rings with chloride-, and bromide-based anions have identical values. Effective negative charges on the nitrogen atoms are virtually identical to chloride-, bromide-, and acetate-based salts which have a 1-methylpyridinium cation. Acetate anion has the greatest negative charge on the O^1 and O^2 atoms. The main calculated parameters of the optimized complexes are presented in Tables 4 and 5 [11].

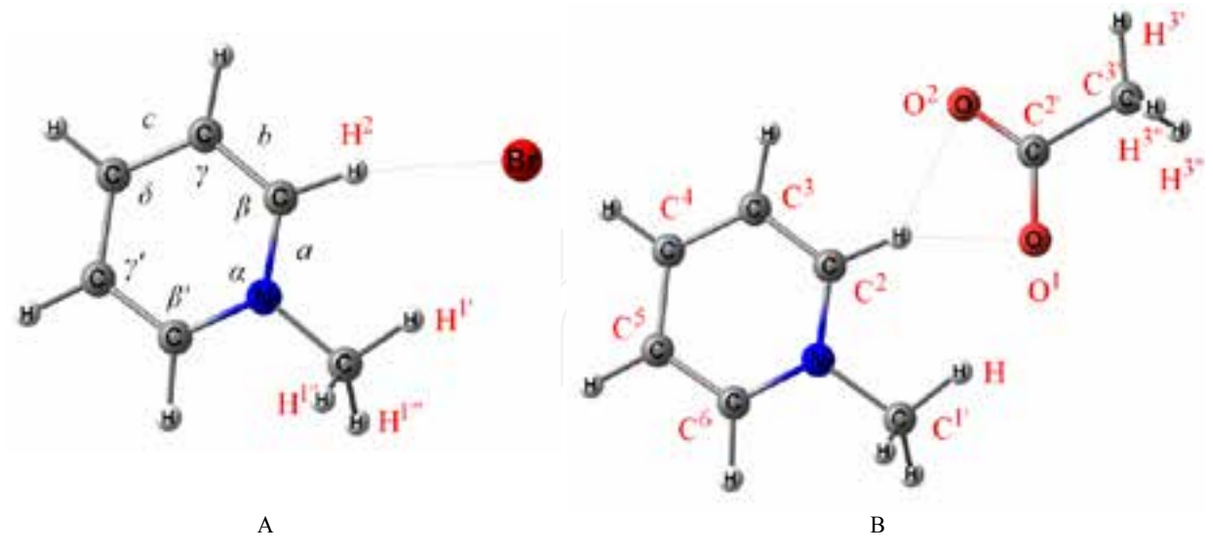

Figure 4. Optimized models of 1-methylpyridinium bromide (A), and 1-methylpyridinium acetate (B)

	Parameters	$[C_1Py]^+$	$[C_1Py]Cl$	$[C_1Py]Br$
Geometry	*a*	1.339	1.331	1.331
	b	1.372	1.387	1.387
	c	1.388	1.374	1.374
	α	120.68	121.36	121.24
	β	121.13	119.95	120.02
	β'	121.13	121.27	121.32
	γ	118.80	119.49	119.48
	γ'	118.80	118.49	118.50
	δ	119.46	119.46	119.43
	$r_{(X...H2)}$		2.191	2.348
	$r_{(X...H1')}$		2.463	2.580
Charges	q_X		-0.852	-0.839
	q_N	-0.655	-0.603	-0.604
	q_{C^2}	0.163	0.185	0.174
	q_{C^3}	-0.271	-0.301	-0.301
	q_{C^4}	-0.087	-0.097	-0.097
	q_{C^5}	-0.271	-0.284	-0.283
	q_{C^6}	0.163	0.156	0.165
	$q_{C^{1'}}$	-0.332	-0.353	-0.356

http://dx.doi.org/10.5772/59286

	Parameters	$[C_1Py]^+$	$[C_1Py]Cl$	$[C_1Py]Br$
	$q_H{}^{2}$	0.311	0.363	0.367
	$q_H{}^{3}$	0.293	0.275	0.275
	$q_H{}^{4}$	0.296	0.248	0.258
	$q_H{}^{5}$	0.293	0.257	0.255
	$q_H{}^{6}$	0.311	0.255	0.266
	$q_H{}^{1'}$	0.236	0.325	0.316
	$q_H{}^{1''}$	0.235	0.206	0.207
	$q_H{}^{1'''}$	0.244	0.206	0.206
E_p			-369.918	-372.344

Table 4. The bond lengths (Å), angles (deg.), interaction energies E_p (kJ mol^{-1}) and atomic charges of 1-methylpyridinium chloride and bromide, calculated by HF/6-31G (d). X=anion [11]

	Parameters	Values
Geometry	*a*	1.328
	b	1.389
	c	1.371
	α	121.37
	β	120.36
	β′	120.91
	γ	119.11
	γ′	118.73
	δ	119.52
	$r_{(O1...H2)}$	1.981
	$r_{(O2...H2)}$	2.045
	angle ($O^1C^{2'}O^2$)	125.59 (110.57)
	$r_{(C2'...C3')}$	1.527
Charges	q_N	-0.603
	$q_C{}^{2}$	0.138
	$q_C{}^{3}$	-0.301
	$q_C{}^{4}$	-0.104
	$q_C{}^{5}$	-0.283
	$q_C{}^{6}$	0.148
	$q_C{}^{1'}$	-0.362

	Parameters	Values
	$q_{C}^{2'}$	0.760 (0.723)
	$q_{C}^{3'}$	-0.554 (-0.554)
	q_{H}^{2}	0.442
	q_{H}^{3}	0.298
	q_{H}^{4}	0.252
	q_{H}^{5}	0.248
	q_{H}^{6}	0.258
	$q_{H}^{1'}$	0.342
	$q_{H}^{1''}$	0.200
	$q_{H}^{1'''}$	0.200
	$q_{H}^{3'}$	0.155 (0.116)
	$q_{H}^{3''}$	0.160 (0.114)
	$q_{H}^{3'''}$	0.155 (0.116)
	q_{O}^{1}	-0.789 (-0.758)
	q_{O}^{2}	-0.759 (-0.758)
	Σ (CH_3COO)	-0.872 (-1.000)
E_p		-418.464

Table 5. Bond lengths (Å), angles (deg.), interaction energies E_p (kJ mol^{-1}) and atomic charges of 1-methylpyridinium acetate, calculated by HF/6-31G (d). (The values of the parameters for isolated acetate-anions are shown in parentheses) [11].

It is important to note that in the series of acetate > chloride > bromide the negative charges of the anion have been decreasing (for acetate-anion is the total value of the charges on the O^1 and O^2 atoms), and it decreases the positive charges on the cations which interact due to the H^2 and $H^{1'}$ atoms with the anions. This is due to a decrease in the electron density transfer during interionic interactions. As a result, in the same series, the interaction energy between the cation and anion decreases, and the distance between the anion and cation increases. In practice, this could be the reason for the decrease in the solubility of the cellulose in these salts. For example, [APy]Cl dissolves in seven times more biomass poplar than [APy]Br (Table 3). It is also important that the imidazolium-based ILs produce similar theoretical and experimental results [22, 27].

3.1.2. Features of the structures of 1,3-disubstituted-pyridinium-based ILs

Figure 5 shows the potential energy surface for the 1,3-disubstituted pyridinium IL from the example of [C_4MPy]Cl. For [C_4MPy]Cl we observed two structures of ion pairs in mutual arrangement. These structures correspond to the minima of E_p: chloride-anion is located near

http://dx.doi.org/10.5772/59286

the protons H^2 (Figure 5, point I) and H^6 (Figure 5, point II). The E_p values of both the cation-anion pairs with variable positions (Figure 6) for these ions are not significantly different.

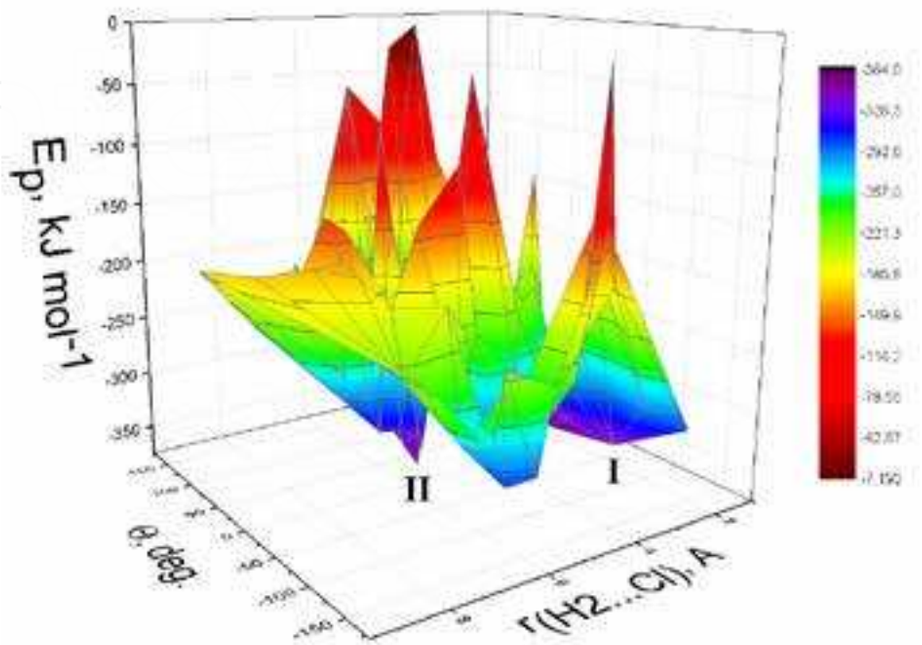

Figure 5. PES for $[C_4MPy]Cl$. The Roman numerals indicate the points of the energy minima on the PES

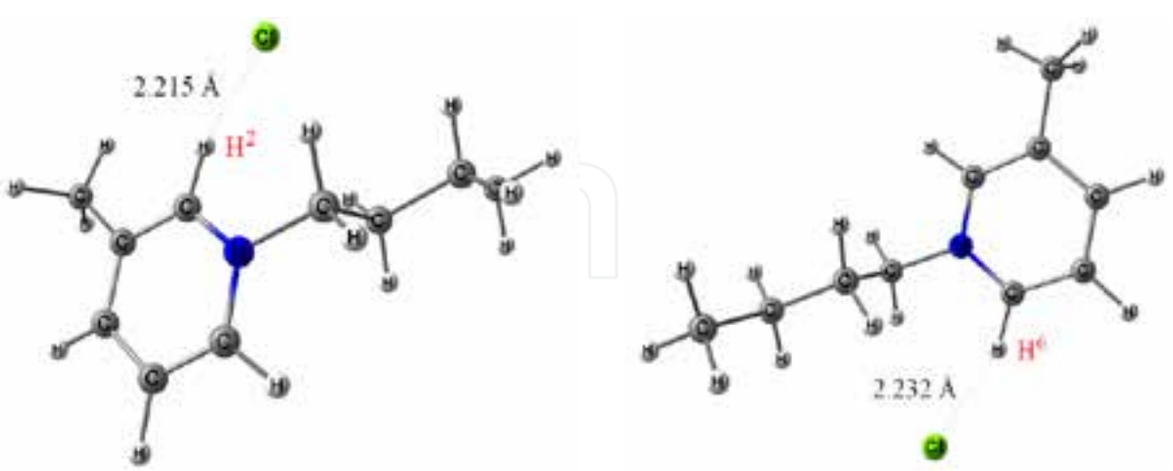

A B

Figure 6. Two optimized models of $[C_4MPy]Cl$: on a PES to point I corresponds to structure A, and for point II – structure B

The results of the quantum chemical calculations for the other IL models give similar geometries with the mutual arrangement of the anion around the cation. The optimized models of $[C_4MPy]CH_3COO$ and $[C_4MPy]Br$ are shown in Figure 7.

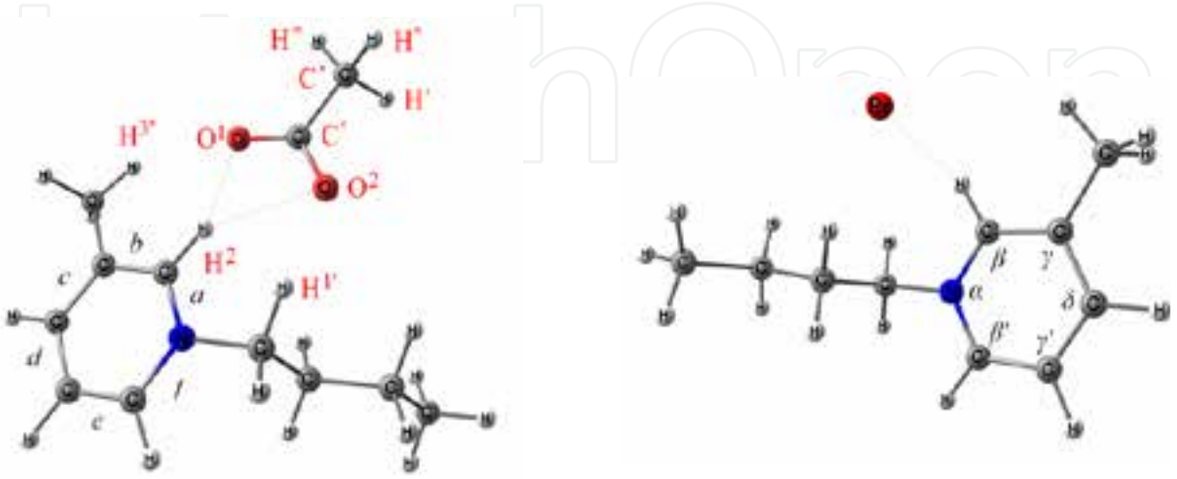

A B

Figure 7. Optimized models of $[C_4MPy]CH_3COO$ (A), and $[C_4MPy]Br$ (B)

Since we observed the global minimum of the potential energy on the PES for the model with the anion located near to the H^2 ring proton, this model was adopted for all subsequent calculations of geometry. The main results of the quantum chemical calculations are shown in Tables 6 and 7. The mutual arrangement of the anion around the cation is characterized by the torsion angle Θ between the anion X, and the pyridinium ring atoms H^2, C^2, and N, and the distance $r_{(H2...X)}$ between the anion X and the H^2 atom. Thus, for 1,3-disubstituted chloride-containing pyridinium models, the torsion angle Θ has a range from 0.2º (for $[C_1MPy]Cl$) to 11.1º and 14.2º (for the substituted pyridinium-based chlorides with chain lengths of C_2 to C_{10}). We can compare, for monosubstituted 1-methylpyridinium chloride the Θ ≈ 0º. The Θ angle for bromide-containing models is 7 – 15º more than the same chloride-based models. Having the anion located further away from the plane of the pyridinium ring, and the increase in the Θ between the cation and anion in the homologous series, and finally the changing of the anion Cl^- to Br^- makes the cation-anion pair still less associated. The reason for this is the reducing of the ion's packing density in the IL crystal, and thus their melting point was changed. A decrease in the degree of the association is also confirmed by a characteristic change in the E_p values. The length of the C—C bonds, and angles with the pyridinium ring for the calculated models in general are not very different from each other. Monosubstituted and disubstituted salts have different geometric parameters: the long distances of *b* and *c*, and the relatively large angles of *α* and *β* have a 1-alkyl-3-methylpyridinium ring relative to the 1-alkylpyridinium ring. These differences are caused by relatively strong interactions with the anions.

http://dx.doi.org/10.5772/59286

ILs	$r_{(H2...X)}$	$r_{(C2...H2)}$	*a*	*b*	*c*	*d*	*e*	*f*	*α*	*β*	*β′*	*γ*	*γ′*	*δ*	Θ	Φ
$[C_1MPy]Cl$	2.182	1.085	1.331	1.391	1.380	1.396	1.363	1.342	121.48	121.20	120.56	117.47	118.76	120.53	0.193	
$[C_2MPy]Cl$	2.192	1.085	1.332	1.389	1.382	1.393	1.366	1.340	121.36	121.30	120.65	117.45	118.74	120.50	11.148	
$[C_3MPy]Cl$	2.213	1.084	1.333	1.388	1.382	1.393	1.366	1.339	121.36	121.31	120.65	117.43	118.73	120.51	10.827	177.687
$[C_4MPy]Cl$	2.215	1.084	1.333	1.388	1.383	1.392	1.366	1.339	121.36	121.32	120.65	117.43	118.74	120.51	13.791	177.768
$[C_5MPy]Cl$	2.216	1.084	1.333	1.388	1.383	1.393	1.366	1.338	121.36	121.32	120.65	117.43	118.74	120.51	13.547	177.479
$[C_6MPy]Cl$	2.216	1.084	1.333	1.388	1.383	1.392	1.367	1.338	121.36	121.32	120.65	117.43	118.73	120.51	14.083	177.477
$[C_7MPy]Cl$	2.216	1.084	1.333	1.388	1.383	1.392	1.366	1.338	121.36	121.32	120.65	117.43	118.74	120.51	14.185	177.482
$[C_8MPy]Cl$	2.216	1.084	1.333	1.388	1.383	1.392	1.367	1.338	121.36	121.32	120.65	117.43	118.74	120.51	14.190	177.479
$[C_9MPy]Cl$	2.216	1.084	1.333	1.388	1.383	1.392	1.367	1.338	121.36	121.32	120.65	117.43	118.73	120.51	14.191	177.496
$[C_{10}MPy]Cl$	2.216	1.084	1.333	1.388	1.383	1.392	1.366	1.338	121.36	121.32	120.65	117.43	118.73	120.51	14.192	177.500
[AMPy]Cl	2.223	1.081	1.329	1.393	1.379	1.396	1.363	1.343	121.40	121.38	120.56	117.39	118.79	120.52	54.890	114.289
$[C_2MPy]Br$	2.335	1.083	1.332	1.388	1.382	1.393	1.366	1.339	121.20	121.52	120.66	117.39	118.81	120.42	26.664	177.256
$[C_4MPy]Br$	2.377	1.082	1.333	1.387	1.383	1.392	1.367	1.338	121.23	121.49	120.66	117.38	118.78	120.45	20.810	175.746
$[C_4MPy]CH_3COO$	1.841*	1.088	1.333	1.389	1.382	1.393	1.366	1.339	121.45	121.12	120.70	117.58	118.72	120.45		177.256

* The distance from the O^1 oxygen atom of acetate-anion to H^2 of pyridinium ring; distance from O^2 to H^2 is 2.526 Å.

Table 6. The main geometrical parameters: bond lengths (Å), and angles (degrees) for 1,3-disubstituted pyridinium salts, calculated by HF/6-31G (d) (An explanation of the symbols is given in the text and in figure 7)

ILs	q_X	q_{H^2}	q_{H^6}	$q_{H^{1'}}$	$q_{H^{3''}}$	q_N	q_R	q_M	μ, D	E_p
$[C_1MPy]Cl$	-0.854	0.356	0.262	0.321	0.253	-0.604	0.381	0.117	15.268	-366.799
$[C_2MPy]Cl$	-0.863	0.357	0.261	0.300	0.251	-0.604	0.401	0.114	14.903	-364.635
$[C_3MPy]Cl$	-0.865	0.359	0.262	0.297	0.249	-0.610	0.409	0.113	14.683	-364.851
$[C_4MPy]Cl$	-0.866	0.360	0.262	0.295	0.249	-0.611	0.411	0.113	14.547	-363.813
$[C_5MPy]Cl$	-0.867	0.360	0.262	0.295	0.249	-0.611	0.412	0.113	14.501	-363.096
$[C_6MPy]Cl$	-0.867	0.360	0.262	0.295	0.249	-0.611	0.412	0.113	14.447	-362.593
$[C_7MPy]Cl$	-0.867	0.360	0.262	0.295	0.249	-0.611	0.412	0.113	14.447	-362.245
$[C_8MPy]Cl$	-0.867	0.360	0.262	0.295	0.249	-0.611	0.412	0.113	14.414	-362.009
$[C_9MPy]Cl$	-0.867	0.360	0.262	0.295	0.249	-0.611	0.412	0.113	14.430	-361.838
$[C_{10}MPy]Cl$	-0.867	0.360	0.262	0.295	0.249	-0.611	0.412	0.113	14.403	-361.719
[AMPy]Cl	-0.871	0.350	0.264	0.307	0.248	-0.607	0.395	0.115	14.622	-362.775
$[C_2MPy]Br$	-0.849	0.363	0.262	0.286	0.249	-0.606	0.390	0.113	15.094	-370.408
$[C_4MPy]Br$	-0.848	0.363	0.263	0.283	0.245	-0.611	0.397	0.112	14.778	-371.665
$[C_4MPy]CH_3COO$	-0.774*	0.443	0.257	0.328	0.267	-0612	0.398	0.104	11.269	-412.003

* A partial charge of the O^1 oxygen atom; partial charges to other atoms of the acetate-anion:-0.749 for O^2, 0.753 for C',-0.556 for C'', 0.160 for H', 0.156 for H'', 0.156 for H''', the total charge of the acetate-anion $q_{(CH_3COO^-)}$ is-0.854e.

Table 7. The partial charges q for atoms and the substituents by the Mulliken value, energy E_p (kJ mol^{-1}) and dipole moments ($\vec{\mu}$) for the models of 1,3-disubstituted pyridinium salts, are calculated by HF/6-31G(d).

For the IL which has an allylic substituent we observed a relatively more larger in the Θ angle relative to $[C_3MPy]Cl$. This may be the result of the interaction of the anion with the π-electrons of the allylic substituent. Because the anion for all of the salts slightly shifted toward the substituent on the nitrogen atom (including $[C_1MPy]Cl$), then in the comparison of these two compounds the closest anion is located in the more polar allylic substituent than the proplic substituent (the distance between the chloride-anion and $H^{1'}$ atom are 2.617 Å and 2.675 Å, respectively). This may indicate a more dense atomic packing for [AMPy]Cl. The Φ angle value for [AMPy]Cl on average is less than the other models.

With respect to the values of the electron density distribution in the ion pair, an increase in the alkyl chain length of the cation clearly affects only the length of C_4. A further increase in the length of the substituent does not lead to significant changes in the charge of the atom H^2. This leads to a decrease in the solvent polarity as a result of increasing the volume portion of the non-polar components. The electric dipole moment $\vec{\mu}$ values, which are characteristic of the electron density asymmetry, are gradually reduced in chloride-containing ILs, where the length of the substituents are increased. The displacement dipole of the moment vector along the alkyl chain length takes place gradually, as shown in Figure 8. The calculated values of μ for bromide-containing ILs are also subject to a similar downward trend of the alkyl chain elongation.

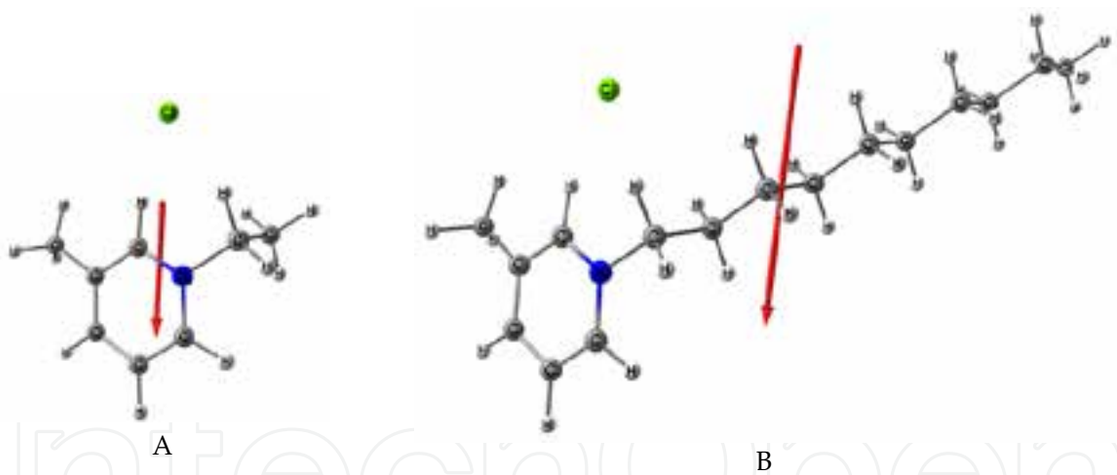

Figure 8. The displacement vector of the dipole moments for $[C_2MPy]Cl$ (A) and $[C_{10}MPy]Cl$ (B)

3.2. Physical and chemical properties of 1-alkyl-3-methylpyridinium-based ILs

A series of 1-alkyl-3-methylpyridinium-based ILs (Table 8) was examined experimentally. The synthesis of these solvents was performed as described in paper [7].

A feature common to most hydrophilic IL crystals (shown in the micrographs on Figure 9) is the gradual saturation of water from the atmosphere. Two of the synthesized ILs, $[C_4MPy]Br$ and $[C_4MPy]CH_3COO$, are liquid at room temperature, i.e. they belong to a subclass RTIL.

http://dx.doi.org/10.5772/59286

No.	ILs	Symbol	M, g mol^{-1}
1	1-Ethyl-3-methylpyridinium chloride	[C_2MPy]Cl	157.6415
2	1-Propyl-3-methylpyridinium chloride	[C_3MPy]Cl	171.6682
3	1-Butyl-3-methylpyridinium chloride	[C_4MPy]Cl	185.6949
4	1-Pentyl-3-methylpyridinium chloride	[C_5MPy]Cl	199.7215
5	1-Hexyl-3-methylpyridinium chloride	[C_6MPy]Cl	213.7482
6	1-Heptyl-3-methylpyridinium chloride	[C_7MPy]Cl	227.7759
7	1-Octyl-3-methylpyridinium chloride	[C_8MPy]Cl	241.8016
8	1-Nonyl-3-methylpyridinium chloride	[C_9MPy]Cl	255.8282
9	1-Decyl-3-methylpyridinium chloride	[C_{10}MPy]Cl	269.8549
10	1-Allyl-3-methylpyridinium chloride	[AMPy]Cl	169.6523
11	1-Ethyl-3-methylpyridinium bromide	[C_2MPy]Br	202.0924
12	1-Butyl-3-methylpyridinium bromide	[C_4MPy]Br	230.1458
13	1-Butyl-3-methylpyridinium acetate	[C_4MPy]CH_3COO	209.2859

Table 8. List of investigated solvents: 1-alkyl-3-methylpyridinium-based ILs, and their molecular weight

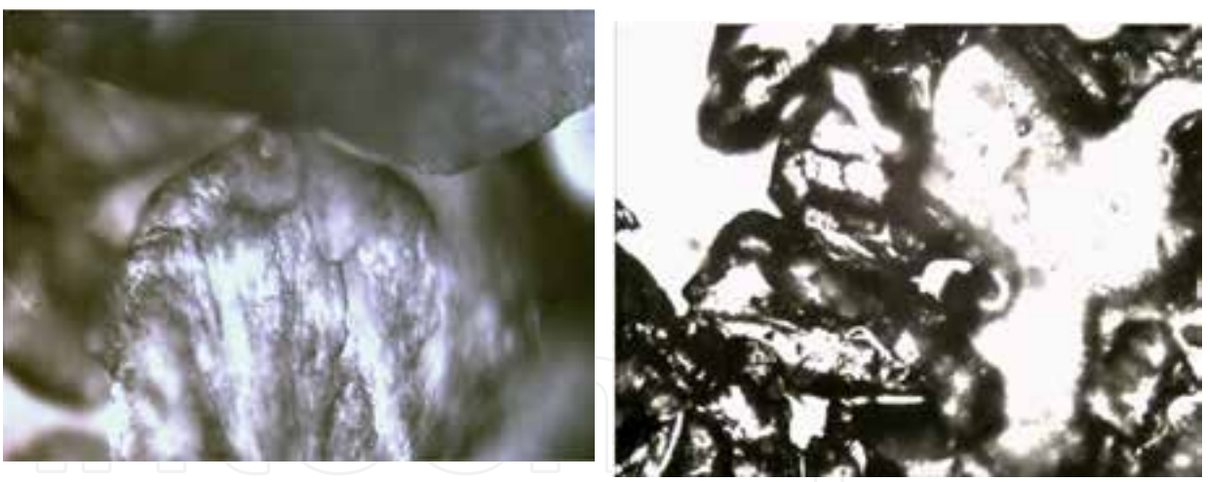

Figure 9. Crystals of [C_2MPy]Cl (A) and [C_4MPy]Cl (B) when magnified 10 times

3.2.1. Study of 1-alkyl-3-methylpyridinium-based ILs by ^{1}H-NMR spectroscopy

The experimental data of the chemical shifts and spin-spin coupling (*J*-couling) are presented in Table 9 [19]. Figure 10 shows the general scheme of the 1-alkyl-3-methylpyridinium ring and acetate-anion numbered to correlate with corresponding the chemical shifts (δ) of protons and proton groups.

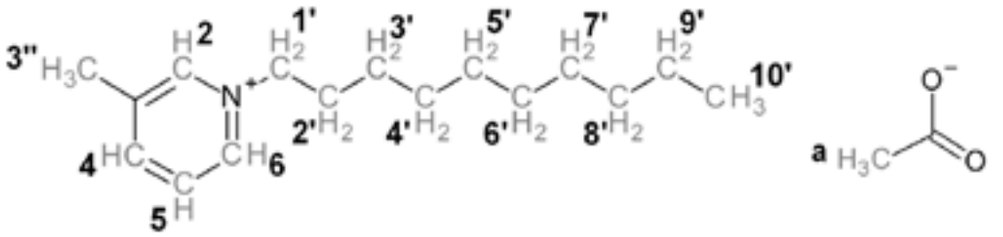

A B

Figure 10. The numbering of the protons and the proton groups for the 1-alkyl-3-methylpyridine cation $[C_nMPy]^+$(A) and the acetate-anion CH_3COO^- (B)

For the peaks of the resonance signals of the ring protons, we observed singlet (H^2), duplet (H^4 and H^6) and triplet (H^5). Here, the *J* for H^4 peak are 7.7 or 8.4 Hz, for H^5 *J*=14, 11.9 or 14.7 Hz (for $[C_4MPy]CH_3COO$), and for H^6 *J*=5.6, 6.3 or 4.2 Hz (for $[C_4MPy]CH_3COO$).

We observed the greatest changes in the values of the chemical shifts during the alkyl chain lengthening for H^2 and H^6 atoms (labelled peaks **2** and **6**, respectively) of the 1-alkyl-3-methylpyridinium ring (to $\Delta\delta$=0.30 and 0.24 ppm, respectively) [19]. According to the quantum-chemical calculations, these provisions in the ion pairs are the most optimal. The changing of the δ value confirms the calculations made on the basis of the findings of the interaction of these atoms with an anion Cl^-, as well as to change the distance between the ion pair in the homologous series of ILs.

With an increase of the alkylic chain length, the δ signals for the H^2 and H^6 atoms begin to move upfield (shielding), while the resonance frequency of the H^4 and H^5 protons are practically unchanged. The upfield δ gives an increase in the distance between the chloride-anion and the corresponding hydrogen atoms of the aromatic ring. For example, according to calculations (see Table 6), the distance $r_{(H2...Cl)}$ for $[C_2MPy]Cl$ is 2.192 Å, and Θ angle=11.148º, whereas $[C_{10}MPy]Cl$ is 2.216 Å, and 14.192º, this corresponds to a change δ^2 of 9.617 ppm to 9.323 ppm.

The replacement of the Cl^--anion with the Br^--anion leads to a significant move upfield for the IL hydrogen atoms. This can be attributed to differences in the effective charges on the atoms and the distances between the cations and the Cl^-/Br^--anions. According to quantum chemical calculations, the $r_{(H2...Cl)}$ distances for some of the chloride-based models are less than the corresponding bromides.

For almost all the pyridinium-based salts, we did not observe any significant changes in $\Delta\delta$ for the hydrogen atoms of the methyl (labelled **3''** and extreme in the ring from **2'** to **10'**) and methylene (except for the extreme groups: from **2'** to **9'**) groups following changes of the alkyl chain length and/or anion species. This indicates the relatively minimal interaction of the anion with the hydrocarbon atoms of the alkyl chain. It may be noted that for [AMPy]Cl, the $H^{3'}$ atom is more upfield shifted in comparison with the same atom for $[C_3MPy]Cl$. These effects can be explained by the greater sensitivity due to the π-electron contribution to the allylic substituent, and the presence of two doublets splitting for the group **3'** from two magnetically inequivalent protons in the *cis*- and *trans*-positions (Figure 11).

http://dx.doi.org/10.5772/59286

ILs	2	3"	4	5	6	1'	2'	3'	4'	5'	6'	7'	8'	9′	10'	a
[C_2MPy]Cl	9.617	2.597	8.182	7.949	9.475	4.974	1.650									
	s	s	d, J=7.7	t, J=14	d, J=6.3	t, J=21.7	t, J=14.7									
[C_3MPy]Cl	9.441	2.601	8.207	7.984	9.353	4.888	2.053	0.959								
	s	s	d, J=7.7	t, J=14	d, J=6.3	t, J=14.7	J=36.4	t, J=14.7								
[C_4MPy]Cl	9.633	2.584	8.192	7.968	9.450	4.928	1.974	1.348	0.880							
	s	s	d, J=7.7	t, J=14	d, J=5.6	t, J=14.7	J=30.1	J=37.8	t, J=14.7							
[C_5MPy]Cl	9.307	2.585	8.211	7.995	9.237	4.869	1.976	1.294		0.817						
	s	s	d, J=7.7	t, J=14	d, J=5.6	t, J=14.7	J=29.4	J=11.2		t, J=14.7						
[C_6MPy]Cl	9.338	2.576	8.205	7.993	9.241	4.855	1.961	1.270	1.197		0.780					
	s	s	d, J=7.7	t, J=14	d, J=5.6	t, J=14.7	J=30.1	J=58.8	J=49.7		t, J=14.7					
[C_7MPy]Cl	9.592	2.579	8.191	7.979	9.394	4.909	1.974	1.292	1.240	1.157		0.760				
	s	s	d, J=7.7	t, J=14	d, J=5.6	t, J=15.4	J=30.1	J=29.4	J=28.7	J=42		t, J=14				
[C_8MPy]Cl	9.566	2.573	8.188	7.979	9.370	4.890	1.966	1.286	1.227	1.142			0.758			
	s	s	d, J=7.7	t, J=14	d, J=5.6	t, J=14.7	J=30.8	J=29.4	J=28.7	J=53.2			t, J=14			
[C_9MPy]Cl	9.488	2.591	8.198	7.987	9.341	4.906	1.978	1.304	1.257	1.186	0.793					
	s	s	d, J=7.7	t, J=14	d, J=6.3	t, J=15.4	J=30.1	J=30.1	J=20.3	J=67.2	t, J=14				0.793	
[C_{10}MPy]Cl	9.323	2.586	8.207	7.992	9.235	4.871	1.966	1.278	1.215	1.178	1.805					1.805
	s	s	d, J=8.4	t, J=13.3	d, J=5.6	t, J=14.7	J=29.4	J=45.5	J=27.3	J=13.3	t, J=14					
[AMPy]Cl	9.473	2.598	8.221	7.962	9.557	5.682	6.123	5.565								
	s	s	d, J=8.4	t, J=14	d, J=6.3	t, J=6.3	J=39.9	d, d								
[C_2MPy]Br	9.510	2.626	8.224	7.972	9.357	5.007	1.697									
	s	s	d, J=8.4	t, J=14	d, J=6.3	t, J=21.7	t, J=14									
[C_4MPy]Br	9.490	2.614	8.236	7.987	9.312	4.924	1.998	1.385	0.917							
	s	s	d, J=7.7	t, J=11.9	d, J=4.2	t, J=14.7	J=28.7	J=37.1	t, J=14.7							
[C_4MPy]CH_3COO	9.198	2.573	8.119	7.928	9.198	4.818	1.934	1.344	0.900							3.540
	s	s	d, J=8.4	t, J=14.7	d, J=4.2	t, J=15.4	J=23.1	J=37.8	t, J=14.7							s

Table 9. Chemical shifts δ (ppm), and spin-spin coupling *J* (Hz) from the ^{1}H-NMR spectra for ILs with $CDCl_3$ [19]

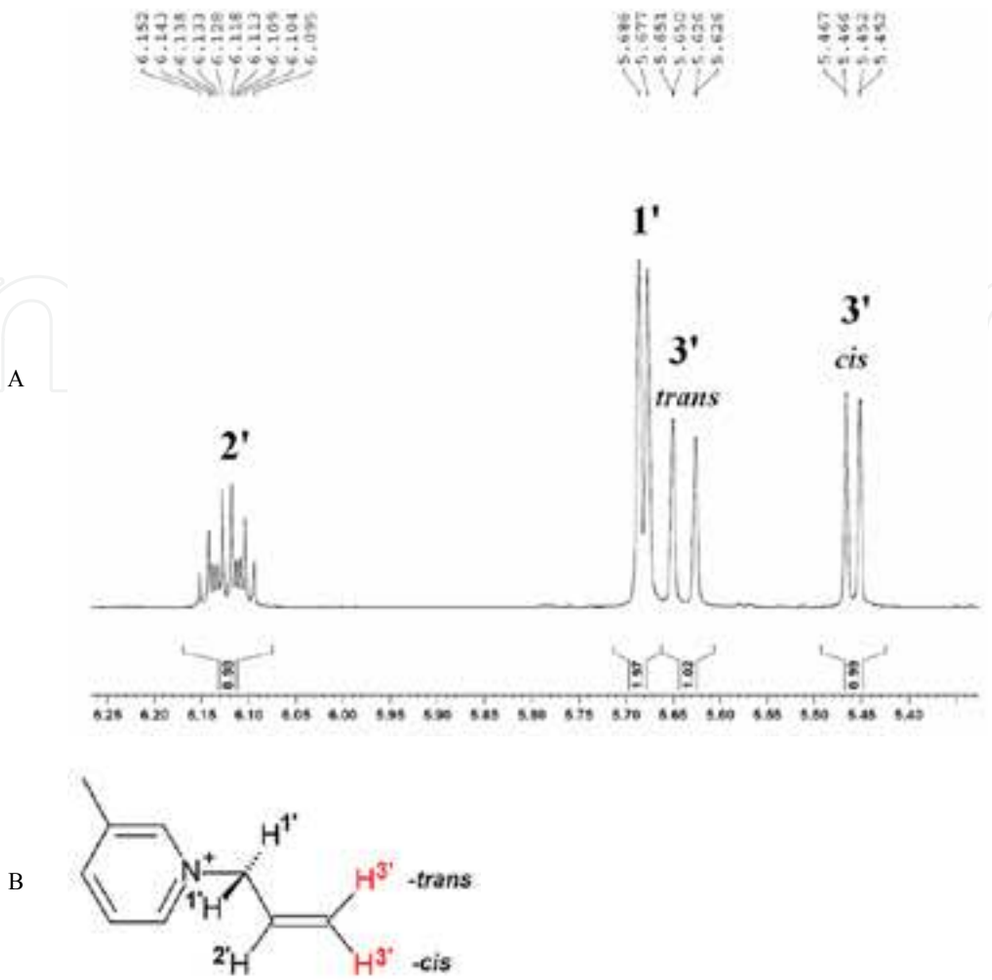

Figure 11. Fragment of the ^{1}H-NMR spectrum, indicating the peaks of the allylic substituent in [AMPy]Cl (A), and the structure of the [AMPy]$^+$ cation (B). Here δ=5.459 (*d*, *J*=10.5 Hz, 1H) – **3'**,*-cis;* δ=5.639 (*d*, *J*=17.5 Hz, 1H) – **3'**,*-trans;* δ=5.682 (*d*, *J*=6.3 Hz, 2H) – **1'**; δ=6.123 (*ddt*, *J*=39.9 Hz, 1H) – **2'**

In this way, the ^{1}H-NMR signals of the spectra for ILs depend strongly on the structure, and this firstly depends on the distances between the cation and anion.

3.2.2. Thermal analysis of 1-alkyl-3-methylpyridinium-based ILs

The phase transition for ILs was investigated using DSC calorimetry and the heated stage [20]. Table 10 shows the melting points and glass transition values for IL.

It should be noted that the glass transition was not revealed for all the ILs. It appeared that the DSC-method was not useful for finding the melting points of some of the ILs, mainly with an odd number of carbon atoms in the alkylic chain. Most of the melting peaks obtained by DSC were not clearly defined. It was impossible to determine the melting point of [C_4MPy]Br by means of DSC, but that IL was a greenish-brown viscous liquid at room temperature, and therefore it could be related to the room temperature ionic liquid (RTIL) species. In contrast, the salt [C_2MPy]Br, due to the high value of its melting point, was not considered as an ionic liquid.

http://dx.doi.org/10.5772/59286

ILs	Glass trans. (DSC)			Melting (DSC)			Melting (Bo.)
	Onset	T_g	Endpt	T_m	Endpt	Ref.	
$[C_2MPy]Cl$	25	29	33				130
$[C_3MPy]Cl$	9	18.5	28				92
$[C_4MPy]Cl$	17	35	53	93	113	95 [4], 111.35 [9]	97
$[C_5MPy]Cl$	16	21.5	27				92
$[C_6MPy]Cl$				62	84	81.95 [9]	77
$[C_7MPy]Cl$	8	16.5	25				72
$[C_8MPy]Cl$				69	83	67.1 [10], 80.05 [9]	74
$[C_9MPy]Cl$							64
$[C_{10}MPy]Cl$				55	82	79.35 [9]	64
[AMPy]Cl	18	27.5	37				108
$[C_2MPy]Br$				146	165		163
$[C_4MPy]Br$							RTIL
$[C_4MPy]CH_3COO$							RTIL

Table 10. ILs glass transition temperature and melting obtained by differential scanning calorimetry (DSC) and use of the Boetius heated stage (Bo.), ºC [20]

In general, it was noticed that there is a tendency that the melting point values of 1-alkyl-3-methylpyridinium chloride-based ILs are reduced with a lengthening of the alkylic chain. This trend could be explained by a decrease in the packing density of the ion pairs of IL following an increase in the number of the alkylic chain carbon atoms.

A complete decomposition of the IL sets is seen at a temperature of about 250 °C [20]. The decomposition temperature values slightly decreased with the growth of the alkylic chain length. Furthermore, again the quaternary pyridinium salts, $[C_2MPy]Cl$ and $[C_3MPy]Cl$, appeared to be the exceptions, as well as with respect to the melting point tendency. A change of the anion ambiguously affected the decomposition temperature, thus $[C_2MPy]Br$ decomposed at a higher temperature than $[C_2MPy]Cl$ but the decomposition temperature of bromides and chlorides with the $[C_4MPy]^+$cation was comparable.

With the use of a gas chromatography-mass spectroscopy, we can identify the fragments resulting from the decomposition $[C_4MPy]Cl$ (at temperatures up to 280 °C). In the chromatogram shown in Figure 12A, there are two significant peaks. Peak 1 (*M*/*Z* 93, 94, Figure 12B) corresponds to 3-methylpyridine, CAS №108-99-6 (with a similarity of 94%). This result is expected, since the 3-methylpyridine is a natural result of the fragmentation of these salts. Peak 2 (*M*/*Z* 150, 151) when compared with the libraries FFNSC 1.2 and NIST08 does not give a satisfactory result. The said peak value may correspond to an isolated cation ($C_{10}H_{16}N$) with a molecular weight of 150.2417 g mol^{-1}. A peak with different *M*/*Z* values is less intense, but the molecular weight can suggest some probable fragments (Figure 13). From the analysis of

Figures 12B and 13, it becomes obvious that the peaks with an *M*/*Z* of less than 79 – 77 may represent fragments of the ILs, formed in the destruction of the pyridinium ring.

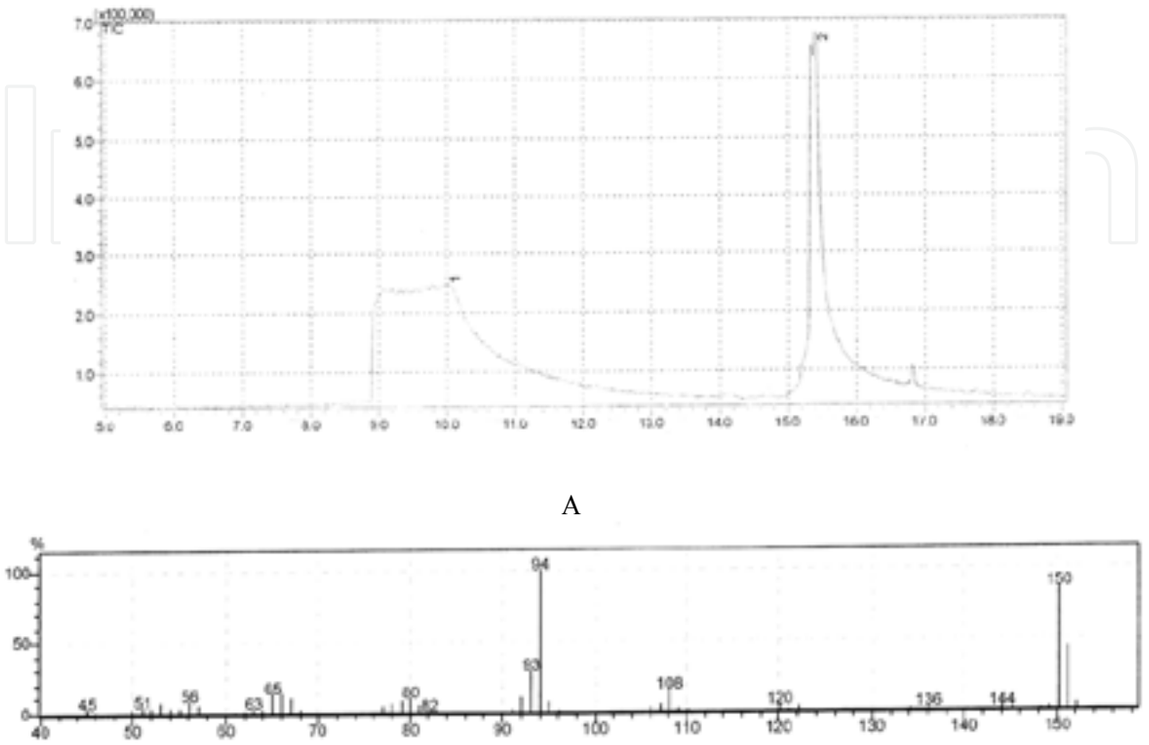

Figure 12. Chromatogram: the function of the time input sample [C_4MPy]Cl, and the values of the detector signal (A); mass spectrum: the *M*/*Z* function and the peaks' intensity (B)

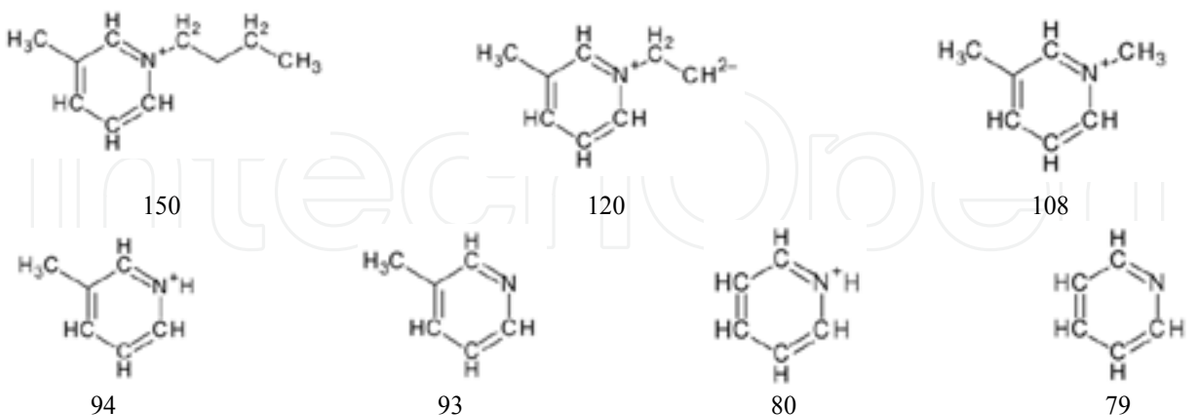

Figure 13. Series of hypothetical fragments formed during the decomposition of [C_4MPy]Cl. Numerals showing the molecular weight of these fragments

Thus, the decomposition fragments of [C_4MPy]Cl are 1-alkyl-3-methylpyridinium cations, 3-methylpyridine, *etc*.

3.2.3. Solvatochromism of 1-alkyl-3-methylpyridinium-based ILs solutions

To determine the Kamlet-Taft hydrogen bond acceptor (basicity, β parameter) for the series of ILs we used indicator [Cu(tmen)(acac)](ClO_4). The obtained data of the β parameter for ILs (from 0.70 to 0.99) indicate a relatively high basicity of the 1-alkyl-3-methylpyridinium-based ILs. More detailed information will published in other works.

4. Dissolution mechanism of cellulose in pyridinium-based ionic liquids

4.1. Dissolution of cellulose with 1-alkyl-3-methylpyridinium-based ILs

Our study of the solubility of cellulose in the synthesized ILs showed that for the same cation the 1-alkyl-3-methylpyridinium bromides show a lower dissolving ability than chlorides, the latter providing more concentrated solutions of cellulose (Table 11). This is consistent with the results of studies on 1-alkyl-3-methylimidazolium halides [7]. An increase in the temperature from 110 to 165 °C leads to a twofold increase in the maximum concentration of cellulose in the solutions of the bromide-containing ILs. With the increasing length of the substituent in the pyridinium chloride ionic liquids, their dissolving power toward cellulose decreases. A similar trend was found for 1-alkylpyridinium [25-29] and 1-alkyl-3-methylimidazolium [27] halides.

ILs	Temperature, °C	D, wt%
[C_2MPy]Cl	140	26
[C_3MPy]Cl	110	22
	120	22.5
[C_4MPy]Cl	120	23
[C_5MPy]Cl	110	21
	120	21
[C_6MPy]Cl	110	19
	120	19
[C_7MPy]Cl	110	14.5
	120	15
[C_8MPy]Cl	110	6.5
	120	8
[C_9MPy]Cl	110	4
	120	5.5
[C_{10}MPy]Cl	110	6

ILs	Temperature, °C	D, wt%
	120	7.5
[AMPy]Cl	130	24
[C_2MPy]Br	165	6.5
[C_4MPy]Br	110	3.5
	165	7
[C_4MIm]Cl	120	17

Table 11. The maximum achieved concentration (D) of cellulose Alicell Super (DP 599) in chloride-and bromide-based ILs [7]

Thus, the results obtained suggest that 1,3-disubstituted pyridinium cation-based ILs are the most effective solvents for cellulose. Pyridinium salt can dissolve in 1.5 times more cellulose than the imidazolium salt with the same substituents and anion. This is confirmed by the data of [4, 6]. We can obtain the 5 – 6 wt% cellulose solutions in [C_2MPy]Cl, [C_3MPy]Cl, [C_4MPy]Cl, [C_5MPy]Cl, [C_6MPy]Cl during 7 – 15 min (Figure 14).

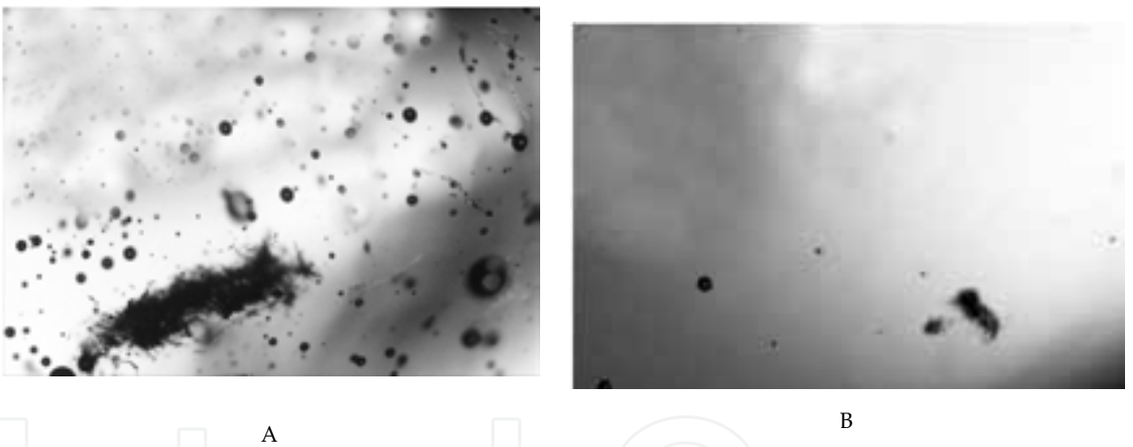

Figure 14. Dissolution of 5 wt% of cellulose with [C_4MPy]Cl for 1 min (A), and 10 min (B) at 120 °C. Increased by four times

The influence of the temperature during the dissolution is accompanied by the degradation of the natural polymer, as exemplified by the reduction in the degree of polymerization (DP) (Table 12).

Dissolution time, min	0	20	120	180
DP	734	419	137	<100

Table 12. DP changing for regenerated cellulose films from their solution in [C_4MPy]Cl at 120 °C, and its influence on dissolution time:

http://dx.doi.org/10.5772/59286

In the FTIR spectra of regenerated cellulose samples of IL, we observed the appearance of characteristic peaks at ~1000 cm^{-1} corresponding predominantly to the C^6H_2–O^6H^6 group. Their presence indicates the modification of cellulose II [30]. For the modification of cellulose I (Alicell Super) stretching vibrations of $\upsilon_{C^6\text{-}O^6}$ were observed at 1031 cm^{-1}. The appearance of two bands at 3440 cm^{-1} and 3484 cm^{-1} (the weak hydrogen bond group of C^2–O^2H^2) also indicate the modification of cellulose II (Figure 15).

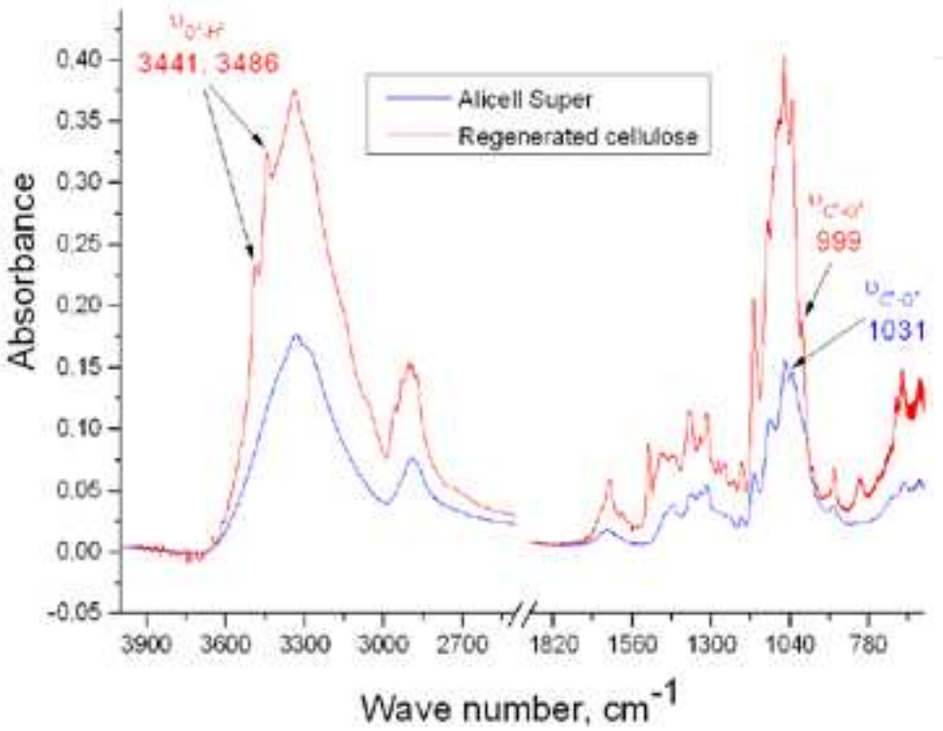

Figure 15. FTIR spectra of Alicell Super and regenerated cellulose from a 23 wt% solution in $[C_4MPy]Cl$

4.2. Study of cellulose solutions with 1-alkyl-3-methylpyridinium-based ILs by ^{1}H-NMR spectroscopy

Table 12 presents ^{1}H-NMR chemical shifts values for cellulose solutions in $[C_4MPy]Cl$ and $[C_4MPy]CH_3COO$. The $\Delta\delta$ values for cellulose varied insignificantly for each of the peaks. We observed the greatest change of $\Delta\delta$ ($\Delta\delta=\delta_{solution} - \delta_{IL}$) for cellulose in $[C_4MPy]Cl$ for H^2 and H^6 protons of the pyridine ring, which shifted upfield. This could be related to the distancing of the anion interacting with the cellulose at the formation of the hydrogen bond. The chemical shifts of H^2 and H^6 changed insignificantly for $[C_4MPy]CH_3COO$ after adding cellulose to the solution. It could be assumed that this was related to the ability of the acetate anion to interact simultaneously with two electron-acceptor centres (cellulose hydroxyls and the IL cation). The δ^a downfield shift of the acetate hydrogen's atoms of the $-CH_3$ group confirmed that the anion of the IL interacted with the cellulose.

ILs	2	4	5	6		
[C_4MPy]Cl	9.573 (-0.060)	8.199 (0.007)	7.977 (0.009)	9.425 (-0.025)		
[C_4MPy]CH_3COO	9.202 (0.004)	8.117 (-0.002)	7.926 (-0.002)	9.202 (0.004)		
A. IL ring protons						
ILs	3''	1'	2'	3'	4'	a
[C_4MPy]Cl	2.601 (0.017)	4.943 (0.015)	1.986 (0.012)	1.367 (0.019)	0.903 (0.023)	
[C_4MPy]CH_3COO	2.569 (-0.004)	4.814 (-0.004)	1.931 (-0.003)	1.340 (-0.004)	0.917 (0.017)	3.780 (0.240)
B. IL protons of –CH_3, and –CH_2 groups						

Table 13. Chemical shifts (δ), taken from the ^{1}H-NMR spectra of cellulose solutions in [C_4MPy]Cl, [C_4MPy]CH_3COO, and their changing Δδ (shown in parentheses) of relative solvents (see Table 9). The solutions were obtained in $CDCl_3$ [19]

Therefore, the interaction of cellulose with pyridinium-based ILs is caused by the ability of the IL anion to exist as the hydrogen bond acceptor.

4.3. Study of the mechanism of cellulose solvation by 1-alkyl-3-methylpyridinium-based ILs using a quantum-chemical calculation

A study of the formation of 'cellulose – ionic liquids' complexes were performed by HF/6-31G(d) quantum-chemical calculation method for the 'cellotetraose – 1-butyl-3-methylpyridinium X' model, wherein X are acetate-, chloride-, and bromide-anions. The geometry of the complexes with optimum energy characteristics are shown in Figure 16.

The formation of the solvate complex is accompanied by the appearance of two hydrogen bonds between the anion and the primary O^6H^6, and the secondary $O^{2'}H^{2'}$ hydroxyl from the neighbouring glycosidic link of the cellotetraose. The distance between the anion and the hydrogen atoms of the cellotetraose hydroxyls, $r_{(H6\text{-}X)}$, $r_{(H2'\text{-}X)}$, ranges from 1.8 to 2.7 Å, and increases in the series of [[C_4MPy]CH_3COO < [C_4MPy]Cl < [C_4MPy]Br.

The geometric characteristics obtained meet the criteria for the formation of the hydrogen bonds [31]: for example, the formation of a hydrogen bond with the chloride-anion has a distance C_{sp^3}–OH···Cl^- in ranges from ~2 Å to ~2.4 Å, and a bond angle (between O, H and Cl) > 140º. The anion of the solvent model is positioned closer to the hydrogen atom of the primary hydroxyl group C^6H_2–O^6H^6.

The interaction of [C_4MPy]Br with the model of the cellulose (Figure 16B), as shown by quantum-chemical calculations, is similar: anion forms hydrogen bonds with both the primary

http://dx.doi.org/10.5772/59286

and secondary hydroxyl groups. The distance between the bromide-anion and the cellotetraose hydroxyl is larger than it is for the chloride-anion (2.445 Å for O^6H^6…Br, 2.710 Å for $O^{2'}H^{2'}$…Br and 2.295 Å for O^6H^6…Cl, 2.514 Å for $O^{2'}H^{2'}$…Cl), because the length of the hydrogen bond between the halide and H-donor increases with the radii of the halide-ions [31].

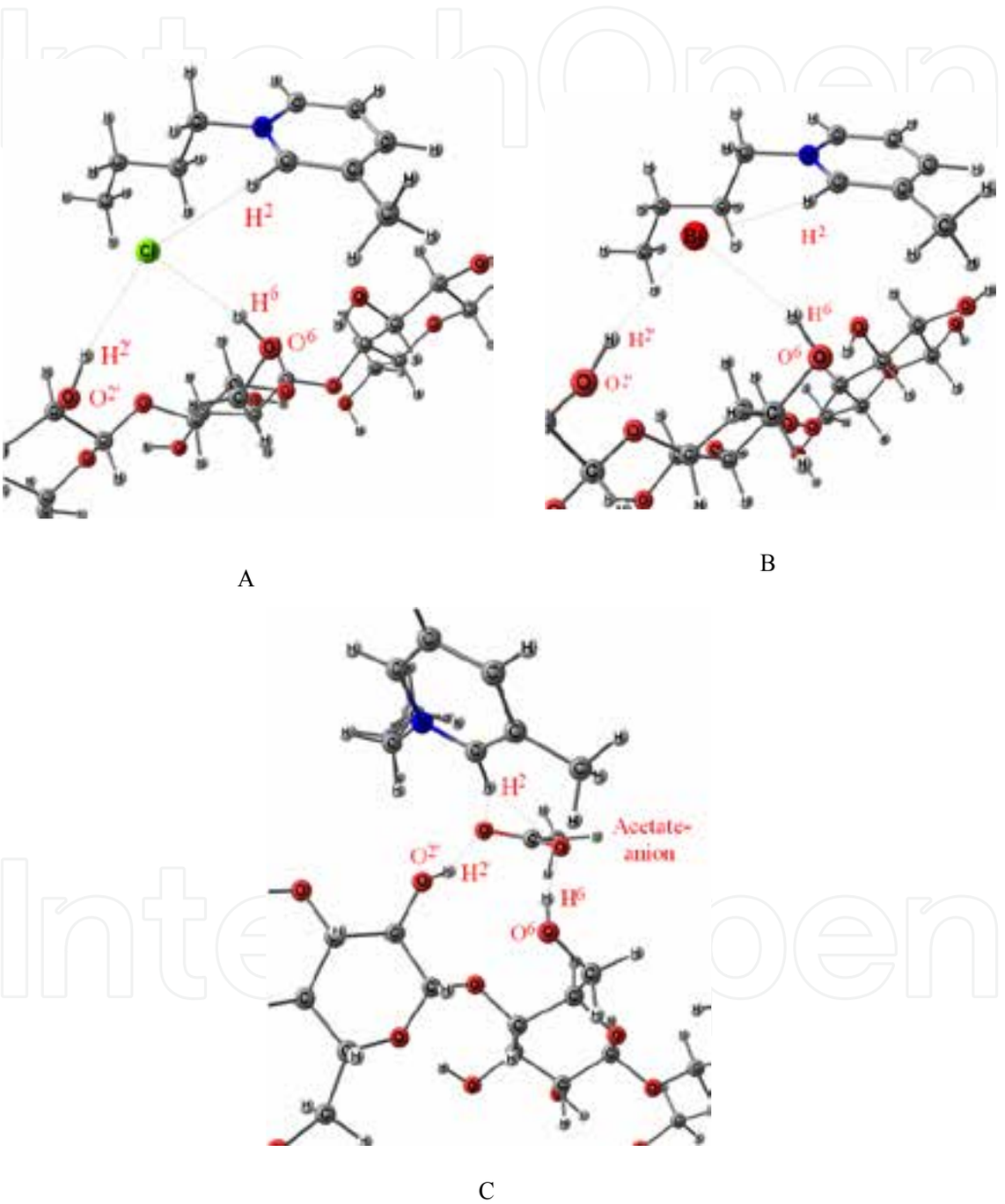

Figure 16. Fragments of optimized complexes of cellotetraose with 1-butyl-3-methylpyridinium chloride (A), bromide (B), and acetate (C)

	Parameters	$[C_4MPy]CH_3COO$	$[C_4MPy]Cl$	$[C_4MPy]Br$
Distances	$r_{(H2...X)}$, Å		2.531 (0.316)	2.640 (0.263)
	$r_{(H2...O1)}$, Å	2.403 (0.562)		
	$r_{(H2...O2)}$, Å	2.252 (-0.274)		
	$r_{(H2'-X)}$, Å	1.853	2.514	2.710
	$r_{(H6-X)}$, Å	1.806	2.295	2.445
Angles	$X–O^{2'}–H^{2'}$, *deg.*	160.17	166.52	167.46
	$X–O^{6}–H^{6}$, *deg.*	165.33	163.94	158.09

Table 14. The main calculated parameters for the solvation complexes of cellotetraose with $[C_4MPy]CH_3COO$, $[C_4MPy]Cl$, and $[C_4MPy]Br$. (In parentheses are the values of the changing parameters relative to the IL pairs, see. Tables 6 and 7)

5. Conclusion

Thus, using quantum-chemical calculations, the features of the interaction of cellulose with 1-alkyl-3-methylpyridinium-based ILs were identified. This shows a decrease in the intensity of the binding of the hydroxyl anions in the series CH_3COO^-, Cl^-, Br^-, which explains the difference in the solvent power of ILs.

According to the theoretical studies (quantum-chemical calculations) and experimental studies (analysis of the chemical shifts), we propose a probable mechanism of the solvation of pyridinium ILs with cellulose, shown in Figure 17.

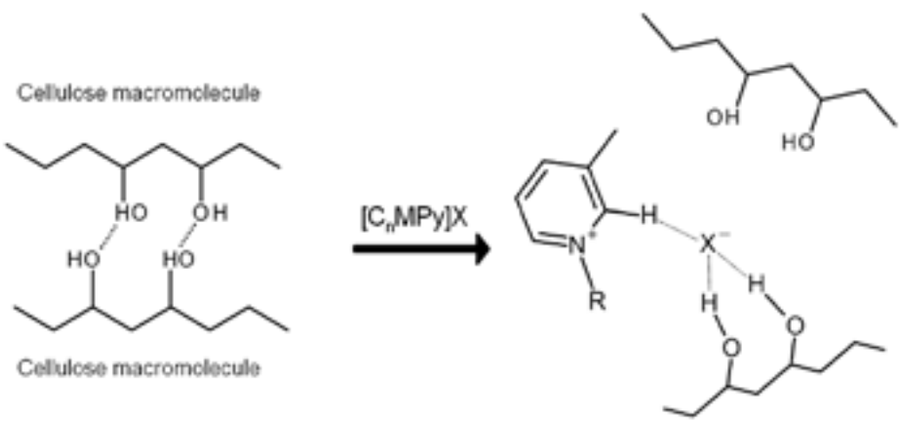

Figure 17. Schematic representation of the interaction mechanism of cellulose with pyridinium-based ILs

In the first stage, the interaction of the polymer with the solvent's anion forms hydrogen bonds with primary and secondary cellulose hydroxyls. The anion maintains ionic bonding with the cation, which at solvation was weakened (the distance between the ions increases).

Acknowledgements

This work was supported by the Ministry of Education and Science of the Russian Federation (State Task No. 2014/186).

Author details

Elena S. Sashina* and Dmitrii A. Kashirskii

*Address all correspondence to: organika@sutd.ru

Institute of Applied Chemistry and Ecology, St. Petersburg State University of Technology and Design, St. Petersburg, Russia

References

[1] Tan S.S.Y., MacFarlane D.R. Ionic Liquids in Biomass Processing, Topics in Current Chemistry 2010; 290 311-339.

[2] da Costa Lopes A.M., Joãoa K.G., Rubik D.F., Bogel-Łukasik E., Duarte L.C., Andreaus J., Bogel-Łukasik R. Pre-treatment of lignocellulosic biomass using ionic liquids: Wheat straw fractionation. Bioresource Technology 2013; 142 198-208.

[3] da Costa Lopes A.M., João K.G., Morais A.R.C., Bogel-Łukasik E., Bogel-Łukasik R. Ionic liquids as a tool for lignocellulosic biomass fractionation. Sustainable Chemical Processes 2013; 1 3.

[4] Heinze T., Schwikal K., Barthel S. Ionic liquids as reaction medium in cellulose functionalization. Macromolecular Bioscience 2005; 5 520-525.

[5] Swatloski R.P., Spear S.K., Holbrey J.D., Rogers R.D. Dissolution of Cellulose with Ionic Liquids. Journal of the American Chemical Society 2002; 124(18) 4974–4975.

[6] Basa M.L.T.N. Ionic Liquids: Solvation Characteristics and Cellulose Dissolution. PhD thesis. University of Toledo; 2010.

[7] Sashina E.S., Kashirskii D.A., Zaborski M., Jankowski S. Synthesis and dissolving power of 1-alkyl-3-methylpyridinium-based ionic liquids. Russian Journal of General Chemistry. 2012; 12(82) 1994-1998.

[8] Harjani J.R., Singer R.D., Garcia M., Scammells P.J. Biodegradable pyridinium ionic liquids: design, synthesis and evaluation. Green Chemistry. 2009; 11 83-90.

[9] Pereiro A.B., Rodriguez A., Blesic M., Shimizu K., Lopes J.N.C., Rebelo L.P.N. Mixtures of Pyridine and Nicotine with Pyridinium-Based Ionic Liquids. Journal of Chemical & Engineering Data. 2011; 56 4356-4363.

[10] Sastry N.V., Vaghela N.M., Macwan P.M., Soni S.S., Aswal V.K., Gibaud A. Aggregation behavior of pyridinium based ionic liquids in water – Surface tension, 1H NMR chemical shifts, SANS and SAXS measurements. Journal of Colloid and Interface Science. 2012; 371 52–61.

[11] Sashina E.S., Kashirskii D.A., Martynova E.V. Features of the molecular structure of pyridinium salts and their dissolving power with respect to cellulose. Russian Journal of General Chemistry. 2012; 4(82) 729-735.

[12] Conceiçao L.J.A., Bogel-Łukasik E., Bogel-Łukasik R. A new outlook on solubility of carbohydrates and sugar alcohols in ionic liquids. RSC Advances 2012; 2 1846-1855.

[13] Zakrzewska M.E., Bogel-Łukasik E., Bogel-Łukasik R. Solubility of Carbohydrates in Ionic Liquids, Energy & Fuels. 2010; 24 737-745.

[14] Sashina E.S., Novoselov N.P., Kuz'mina O.G., Troshenkova S.V. Ionic liquids as new solvents of natural polymers, Fibre Chemistry. 2008; 3(40) 270-277.

[15] Kuzmina O.G., Sashina E.S., Novoselov N.P., Zaborski M. Blends of cellulose and silk fibroin in 1-buthyl-3-methylimidazolium chloride based solutions. Fibres & Textiles in Eastern Europe. 2009; 6(77) 36-39.

[16] Cho C., Jeon Y., Pham T.P.T., Vijayaraghavan K., Yun Y. The ecotoxicity of ionic liquids and traditional organic solvents on microalga Selenastrum capricornutum. Ecotoxicology and Environmental Safety. 2008; 71 166–171.

[17] Couling D.J., Bernot R.J., Docherty K.M., Dixona J.N.K., Maginn E.J. Assessing the factors responsible for ionic liquid toxicity to aquatic organisms via quantitative structure–property relationship modeling. Green Chemistry. 2006; 8 82-90.

[18] Docherty K.M., Kulpa C.F. Toxicity and antimicrobial activity of imidazolium and pyridinium ionic liquids. Green Chemistry. 2005; 7 185-189.

[19] Sashina E.S., Kashirskii D.A., Jankowski S. PMR study of structural features of ionic liquids based on 1-alkyl-3-methylpyridinium and mechanism of their interaction with cellulose. Fibre Chemistry. 2014; 5(45) 268-273.

[20] Sashina E.S., Kashirskii D.A., Janowska G., Zaborski M. Thermal properties of 1-alkyl-3-methylpyridinium halide-based ionic liquids. Thermochimica Acta. 2013; 568 185-188.

[21] Krygowski T.M., Szatyłowicz H., Zachara J.E. How H-bonding Modifies Molecular Structure and π-Electron Delocalization in the Ring of Pyridine/Pyridinium Derivatives Involved in H-Bond Complexation. The Journal of Organic Chemistry. 2005; 70 8859-8865.

[22] Sashina E.S., Novoselov N.P. Effect of structure of ionic liquids on their dissolving power toward natural polymers. Russian Journal of General Chemistry. 2009; 6(79) 1057-1062.

[23] Zherenkova L.V., Komarov P.V., Pavlov A.S. A polymer in an ionic liquid: Structural properties of a system during attraction between the polymer and cations of the ionic liquid. Polymer Science Series A. 2010; 8(52) 864-871.

[24] Klots T.D., Emilsson T., Ruoff R.S., Gutowsky H.S. The Journal of Physical Chemistry. 1989; 93(4) 1255–1261.

[25] Holm J., Lassi U. Ionic Liquids in the Pretreatment of Lignocellulosic Biomass. In: Kokorin A. (ed.) Ionic Liquids: Applications and Perspectives. Rijeka: InTech; 2011. p529-544. Available from http://www.intechopen.com/books/ionic-liquids-applications-and-perspectives/ionic-liquids-in-the-pretreatment-of-lignocellulosic-biomass (accessed 21 February 2011).

[26] Cellulose solution – United States Patent 1943176/ Charles, Graenacher Publication Date: 01.09.1934.

[27] Aerov A.A., Khokhlov A.R., Potemkin I.I. Why Ionic Liquids Can Possess Extra Solvent Power. The Journal of Physical Chemistry B. 2006; 33(110) 16205-16207.

[28] Park T.-J., Murugesan S., Linhardt R.J. Cellulose composites prepared using ionic liquids (ILs)-Blood Compatibility to Batteries. In: Edgar K.J., Heinze T., Buchanan C.M. (ed.). ACS Symposium Series: Polysaccharide Materials: Performance by Design. Washington: American Chemical Society; 2009. p.133-152.

[29] Bentivoglio G., Röder T., Fasching M., Buchberger M., Schottenberger H., Sixta H. Cellulose processing with chloride-based ionic liquids. Lenzinger Berichte. 2006; 86 154-161.

[30] Maréchal Y., Chanzy H. The hydrogen bond network in Iβ cellulose as observed by infrared spectrometry. Journal of Molecular Structure. 2000; 523 183-196.

[31] Bernet B., Vasella A. Intra-and Intermolecular H-Bonds of Alcohols in DMSO, 1H-NMR Analysis of Inter-Residue H-Bonds in Selected Oligosaccharides: Cellobiose, Lactose, N,N′-Diacetylchitobiose, Maltose, Sucrose, Agarose, and Hyaluronates. Helvetica Chimica Acta. 2000; 9(83) 2055-2071.